A novel water index for urban high-resolution eight-band WorldView-2 imagery

Cong Xie, Xin Huang, Wenxian Zeng & Xing Fang

Published online: 22 Apr 2016.

Submit your article to this journal

Article views: 381

View related articles

View Crossmark data

Citing articles: 12 View citing articles

A novel water index for urban high-resolution eight-band WorldView-2 imagery

Cong Xie[a], Xin Huang[b], Wenxian Zeng[c] and Xing Fang[c]

[a]State Key Laboratory of Information Engineering in Surveying, Mapping and Remote Sensing (LIESMARS), Wuhan University, Wuhan, People's Republic of China; [b]School of Remote Sensing and Information Engineering, Wuhan University, Wuhan, People's Republic of China; [c]School of Geodesy and Geomatics, Wuhan University, Wuhan, People's Republic of China

ABSTRACT

Land surface water mapping is one of the most important remote-sensing applications. However, water areas are spectrally similar and overlapped with shadow, making accurate water extraction from remote-sensing images still a challenging problem. This paper develops a novel water index named as NDWI-MSI, combining a new normalized difference water index (NDWI) and a recently developed morphological shadow index (MSI), to delineate water bodies from eight-band WorldView-2 imagery. The newly available bands (e.g. coastal, yellow, red-edge, and near-infrared 2) of WorldView-2 imagery provide more potential for constructing new NDWIs derived from various band combinations. Through our testing, a new NDWI is defined in this study. In addition, MSI, a recently developed automatic shadow extraction index from high-resolution imagery can be used to indicate shadow areas. The NDWI-MSI is created by combining NDWI and MSI, which is able to highlight water bodies and simultaneously suppress shadow areas. In experiments, it is shown that the new water index can achieve better performance than traditional NDWI, and even supervised classifiers, for example, maximum likelihood classifier, and support vector machine.

1. Introduction

Surface water is among the most active and natural earth resources and its changes in time and space have a profound impact on natural systems and human societies (Famiglietti and Rodell 2013). However, water resources are undergoing great changes as a consequence of climate changes and human activities. Therefore, the accurate retrieval and monitoring of surface water is thus crucial for environmental research as well as for the management of terrestrial ecosystems. Mapping accurately surface water (Carroll et al. 2009; Feng et al. 2015; Liao et al. 2014) and monitoring timely its dynamic changes are topics of academic study in a wide range of scientific fields (Craglia et al. 2012).

Remote sensing, as a timely and rapid Earth Observation technique, has become an essential source of information in surface water and other environmental research. Delineation of water areas is one of the most important applications of remote sensing, which is significant to water resource management, flood disaster assessment, and wetland monitoring. Various methods have been developed to delineate surface water from optical remote-sensing images, which can be divided into four common categories (Feyisa et al. 2014; Ji, Zhang, and Wylie 2009): (a) single-band thresholding (Bryant and Rainey 2002; Jain et al. 2005), (b) multi-band spectral index (Feyisa et al. 2014;

McFeeters 1996; Xu 2006), (c) thematic classification (Li and Narayanan 2003; Lira 2006), and (d) linear unmixing (Rogers and Kearney 2004). Moreover, investigators have made efforts to improve the accuracy of water extraction by incorporating these different types of methods (Jiang et al. 2014; Sun et al. 2012). In general, the single-band thresholding method and spectral water index are commonly used for delineating water features due to these methods can be calculated simply and conveniently (Ryu, Won, and Min 2002).

The spectral water index is designed to highlight water features and suppress non-water information, and thus can separate water from non-water by selecting an appropriate threshold value. A simple two-band ratio method has been commonly used for water extraction from remote-sensing images, such as normalized difference water index (NDWI) (McFeeters 1996), which utilizes the normalized ratio of green and near-infrared (NIR) bands to delineate water features. To suppress the noise from built-up areas, Xu (2006) introduced another water index named modified NDWI (MNDWI) by replacing NIR band with shortwave-infrared (SWIR) band on the basis of NDWI. However, the selection of an optimal threshold value for the two-band water indexes is a time-consuming task. Therefore, a multi-band water index named automated water extraction index (AWEI) is introduced to provide robust water extraction accuracies with stable threshold values under various environmental conditions (Feyisa et al. 2014).

In recent years, availability of high-spatial resolution satellite images makes it possible to accurately extract water areas. However, most of the high-spatial resolution remotely sensed images have only four bands (blue, green, red, and NIR), and the SWIR channel used to compute MNDWI or AWEI is not provided. In this context, WorldView-2, a new eight-band high-resolution sensor, is able to provide additional spectral channels (e.g. coastal, yellow, red-edge, and NIR2), where in particular the coastal band is sensitive to water areas (Puetz, Lee, and Olsen 2009) and has the potential for water research and bathymetric studies. Consequently, the four new bands are able to provide more potential to construct more effective water indexes compared to the traditional ones (Wolf 2012). In addition, image classification method is also used to extract water area from high-resolution remote-sensing images. An iterative method by constructing adaptive segmented buffers was developed to delineate water body from urban high-resolution imagery (Zhou et al. 2012). An object-based rule set method combining spectral, geometric, and textural features was employed to extract water body from WorldView-2 imagery and achieved satisfactory water extraction results (Chen et al. 2013). However, the selection of an appropriate parameter for image segmentation is a time-consuming task, which has an important impact on the object-oriented water extraction result.

More importantly, although progresses have been achieved for water extraction, the confusion between shadow and water, due to their similar spectral reflectance, is a pending problem for both high-resolution images (Nath and Deb 2010; Luo et al. 2010; Zhou et al. 2012) and moderate- and low-resolution images (Feyisa et al. 2014; Jiang et al. 2014; Li, Zhang, and Shen 2013). To our knowledge, there is no existing water index proposed for high-resolution remote-sensing data, which can extract water information and at the same time suppress the false alarm of shadow. Thus, the objective of this paper is to develop a novel water index for WorldView-2 imagery by integrating the optimized NDWI model by using the morphological shadow index (MSI; Huang and Zhang 2012), which is able to eliminate the shadow information.

The contributions of this study lie in two aspects: (1) to test the performances of different NDWI models constructed by all possible combinations of WorldView-2 bands, and (2) to create a new water index (NDWI-MSI) for WorldView-2 imagery, based on the optimized NDWI model and shadow removal.

2. Study areas and data

The study areas are located in the three typical mega cities (i.e. Shenzhen, Hangzhou, and Wuhan) of China (Figure 1). The cities have abundant water resources including rivers, lakes, reservoirs, and
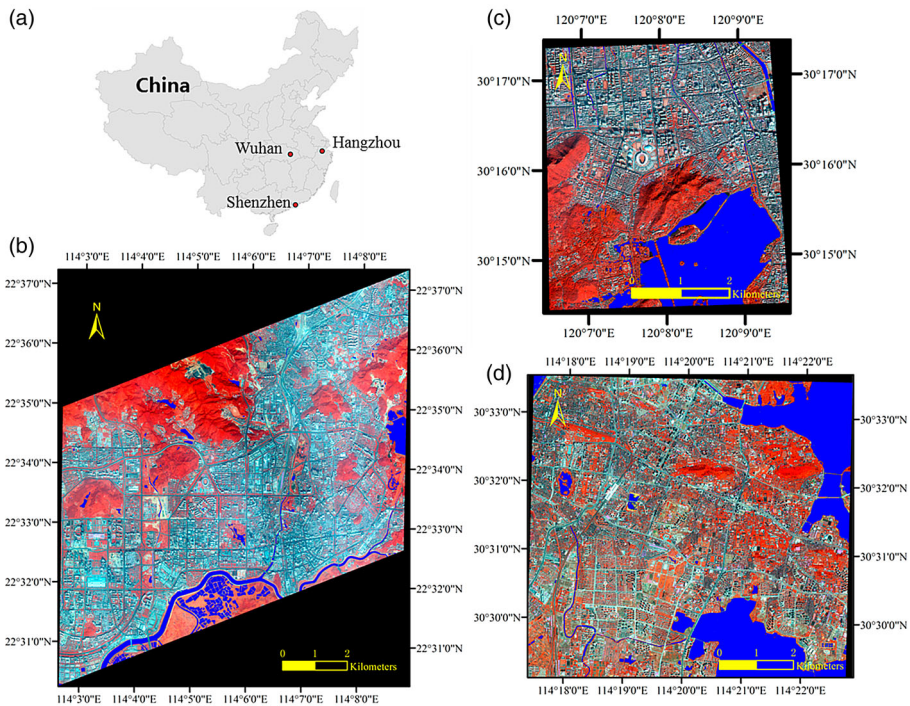
Figure 1. (a) Location of the study areas in China; (b), (c), and (d) are WorldView-2 false color images (8, 3, and 2) overlaid with ground truth references covering Shenzhen, Hangzhou, and Wuhan, respectively.

ponds. The urban areas consist of complex urban features such as built-up areas, vegetation, bare land, and shadow, which are suitable and challenging to test the performance and robustness of the proposed water index.

In this study, three WorldView-2 images over the urban areas were used for water extraction to test the robustness of the proposed method. The detailed parameters of the three images are provided in Table 1. Figure 1 shows the images as well as the corresponding ground truth references of the study areas. The ground truth maps were delineated manually based on careful visual interpretation and a field campaign.

3. Methodology

3.1. Water indexes

NDWI (McFeeters 1996) has been widely used to delineate water areas from remote-sensing images. NDWI is designed according to the difference of spectral response between green and NIR channels,

Table 1. Parameters of the three WorldView-2 images.

Study area	Acquisition date	Wavelength (nm)	Spatial resolution (m)	Image size (pixel)
Shenzhen Hangzhou Wuhan	3 November 2010 Not available 26 April 2012	Coastal: 400–450 Blue: 450–510 Green: 510–580 Yellow: 585–625 Red: 630–690 Red-edge: 705–745 NIR1: 770–895 NIR2: 860–1040	2.0	6433 × 5409 2750 × 2454 4179 × 4369

considering the strong absorption of NIR by water features and the high reflectance of NIR by vegetation and soil features (Xu 2006). Therefore, NDWI is defined as the normalized ratio of the relatively high-reflective band (ρ_h) and the low-reflective band (ρ_l):

$$\text{NDWI} = \frac{\rho_h - \rho_l}{\rho_h + \rho_l}. \tag{1}$$

WorldView-2 imagery with eight spectral bands (especially newly added four bands) can provide a new perspective for constructing different NDWIs. To maximize the potential of the eight-band imagery, four p_h bands (coastal, blue, green, and yellow) and three p_l bands (red-edge, NIR1, and NIR2), as well as their respective average values (avg1 (Equation (2)) and avg2 (Equation (3))), are selected to compute the possible two-band combinations of water indexes for the WorldView-2 image. Hence, $5 \times 4 = 20$ NDWI indexes as well as the sum of all NDWIs (NDWI_sum in Equation (4)) can be computed from the WorldView-2 images (Table 2).

$$\text{avg1} = \frac{\text{coastal} + \text{blue} + \text{green} + \text{yellow}}{4}, \tag{2}$$

$$\text{avg2} = \frac{\text{red - edge} + \text{NIR1} + \text{NIR2}}{3}, \tag{3}$$

$$\text{NDWI\_sum} = \sum_{i}^{n} \text{NDWI}_i, \tag{4}$$

where NDWI_i indicates the ith NDWI and n is the number of water indexes.

3.2. Morphological Shadow Index

In this study, in order to efficiently suppress the false alarms of shadow areas, MSI (Huang and Zhang 2012), a recently developed automatic shadow detector for high-resolution imagery, is applied to enhance the traditional NDWI. MSI is constructed by describing the spectral-spatial properties of shadow using a series of morphological operations. The calculation of MSI is based on the fact that the relatively low spectral reflectance of shadows and the spatially adjacent buildings can lead to a high local contrast of shadows. The calculation steps of the MSI are briefly described as follows.

Step 1. Calculation of brightness: the brightness image b is generated by recording the largest value of each pixel in the available channels, since shadow is dark and has low response in all the spectral bands.

Step 2. Black top-hat by reconstruction (BTH): It is defined as:

$$\text{BTH}(d, s) = \varphi_b^{re}(d, s) - b, \tag{5}$$

where $\text{DMP}_{\text{BTH}}(d, s) = |\text{BTH}(d, (s + \Delta s)) - \text{BTH}(d, s)|$ is the closing-by-reconstruction filter, s and d indicate the length and direction of a linear structuring element (SE), respectively.

Step 3. Differential morphological profiles (DMPs):

$$\text{DMP}_{\text{BTH}}(d, s) = |\text{BTH}(d, (s + \Delta s)) - \text{BTH}(d, s)|, \tag{6}$$

Table 2. All possible water indexes for WorldView-2 imagery.

| Water indexes	ρ_h	ρ_l	Num.
NDWIs	Coastal, blue, green, yellow, avg1	Red-edge, NIR1, NIR2, avg2	20
NDWI_sum		$\text{NDWI\_sum} = \sum_{i}^{n} \text{NDWI}_i$	1

where DMP_{BTH} can be viewed as a shape spectrum (Huang and Zhang 2012) used to highlight the dark structures in different scales ($s_{min} \leq s \leq s_{max}$) and directions. Δs is the interval of the scales in the profiles.

Step 4. Calculation of the MSI:

$$MSI = \frac{\sum_{d,s} DMP_{BTH}(d, S)}{D \times S}, \tag{7}$$

where D and S indicate the number of directions and scales for the profiles, respectively. MSI is defined as the mean of the DMP_{BTH} profiles since shadow shows large BTH values in different scales and directions. Consequently, shadow areas correspond to large MSI feature values. Readers can refer to Huang and Zhang (2012) for details about MSI.

The directions ($D = 4$) of the linear SE were set to 0°, 45°, 90°, and 135° in this paper since our previous study showed that increase of value of D does not signify improvement of shadow detection (Huang and Zhang 2012). The scale parameters (s_{min}, s_{max}, and Δs) were set to (2, 52, and 5) according to the spatial resolution (2 m) of images. However, it is actually difficult to choose a suitable value of s for complex high-resolution urban scenes, since a low value is subject to omission of shadow (see the box in Figure 2(b)) but a high value may lead to wrong extraction of small-area water bodies (see the box in Figure 2(c)). Consequently, an appropriate strategy is to define a large value of s_{max} and then refine the result using shape (e.g. density) and texture features (e.g. homogeneity) to eliminate these
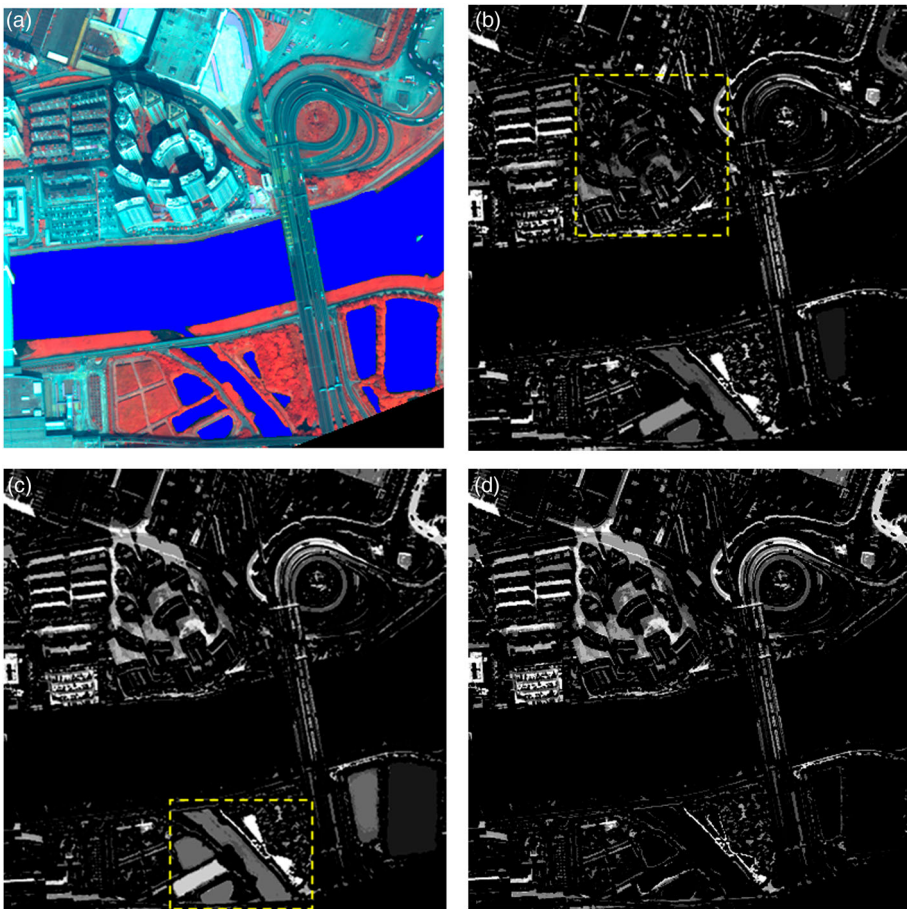
Figure 2. An example showing the results of MSI: (a) is an example image overlaid with reference, (b) and (c) are the MSI feature images, with the sizes of SE (s_{min}, s_{max}, and Δs) set as (2, 22, and 5) and (2, 52, and 5), respectively, and (d) is the refined result of (c).

wrongly detected objects from the MSI feature image (Figure 2(d)). It should be noted that homogeneity derived from the gray-level co-occurrence matrix is used to eliminate the small-area water bodies by manually setting the threshold value as .1 considering the texture of water is more homogeneous than shadow. The density feature is used to remove the elongated water bodies (e.g. rivers) using the threshold value of .7 since elongated structures are related to lower density value.

3.3. The Proposed Water Index

We can find an optimized band combination for the NDWI defined in Equation (1), based on the eight-band WorldView-2 imagery. Subsequently, the residual shadow can be further suppressed by considering the shadow index introduced previously. As shown in Figure 3, in this study, a new water index combining NDWI and MSI is proposed to accurately delineate water areas from WorldView-2 imagery. The calculation procedure of the proposed water index consists of the following three steps:

(1) calculation of the optimized NDWI ($NDWI_{optimal}$), selected among all the possible band combinations of the eight-band WorldView-2 imagery;
(2) refined MSI for shadow extraction;
(3) calculation of the proposed water index for WorldView-2 ($NDWI_{WV-2}$), by subtracting the shadow components (MSI) from the optimized NDWI:

$$NDWI_{WV-2} = NDWI_{optimal} - MSI, \tag{8}$$

where the values of $NDWI_{optimal}$ and MSI are linearly scaled to [0, 1].
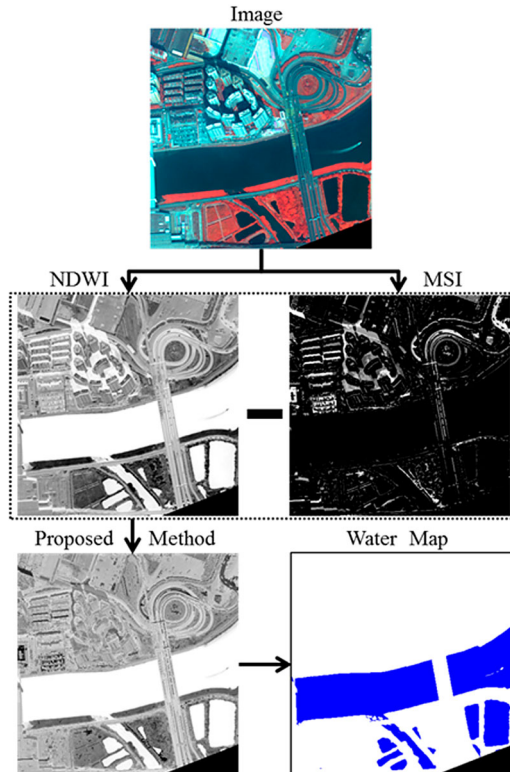

Figure 3. Graphical example of the proposed method.

3.4. Supervised classification methods

To compare the performance of the new index with classification methods, two supervised classifiers including maximum likelihood classifier (MLC) and support vector machine (SVM) were used for water extraction in this study. A brief description of the two classifiers is given as follows.

MLC is a parametric classifier which is commonly used for classification of remotely sensed images. The principle of MLC is based on the assumptions that the input data are Gaussian (normally) distributed, and the distance between a pixel value and a scaled and variance/covariance-corrected class mean is calculated to obtain the probability that the pixel belongs to one of possible classes (Strahler 1980). In contrast to other parametric classifiers, MLC has the advantage of dealing with normally distributed data.

SVM is one of the most popular machine learning algorithms for supervised classification, which is developed based on the statistical learning theory and structural risk minimization principle (Chapelle, Haffner, and Vapnik 1999). SVM has a high generation performance and can be applicable to process the high-dimensional data with small training sample set (Gotsis, Chamis, and Minnetyan 2004). SVM has been reported to achieve better performance than the traditional classification methods (Huang, Davis, and Townshend 2002). However, the choice of the kernel and its parameters has a significant impact on the output results of SVM. In this study, a grid-search technique using fivefold cross-validation is employed to find the optimal kernel function parameters for SVM.

4. Result analysis and validation

The experiments were conducted on the three WorldView-2 images covering Shenzhen, Hangzhou, and Wuhan, respectively. The producer's accuracy (PA), user's accuracy (UA), and Kappa coefficient calculated by confusion matrix were used to evaluate the accuracy of water extraction. The threshold values for water indexes were selected by the receiver operator characteristics curves (Nettleman 1988), which were drawn with the true positive rate (TPR) on the y axis and the false positive rate (FPR) along the x axis. TPR (also called sensitivity or recall) denotes the proportion of the actual water pixels which have been correctly retrieved, while FPR (also called false alarm rate) is the proportion of the actual non-water pixels that have been incorrectly classified as water (Fawcett 2006). The both TPR and FPR values are distributed in [0, 1], which can be defined as Equations (9) and (10), respectively. The goal of our experiments is to achieve the values of high TPR and low FPR. The optimal threshold value can be selected as the tangential point of the curve, indicating a trade-off of TPR and FPR.

$$\text{TPR} = \frac{\#\ of\ true\ detected\ water\ pixels}{total\ \#\ of\ water\ pixels}. \tag{9}$$

$$\text{FPR} = \frac{\#\ of\ false\ detected\ water\ pixels}{total\ \#\ of\ non\text{-}water\ pixels}. \tag{10}$$

Accuracy scores of various NDWIs constructed by different band combinations for Shenzhen WorldView-2 imagery are shown in Table 3. It can be seen that the traditional NDWI (based on green and NIR1 bands, $\text{NDWI}_{\text{green-NIR1}}$) gives the Kappa coefficient of .559. The Kappa value of the NDWI computed by coastal and NIR2 ($\text{NDWI}_{\text{coastal-NIR2}}$) is .669, which outperforms other NDWIs in terms of the accuracy. Table 4 presents the accuracies of water extraction for Hangzhou WorldView-2 data, and it can be seen that the $\text{NDWI}_{\text{coastal-NIR2}}$ as well as the NDWI constructed by green and NIR2 ($\text{NDWI}_{\text{green-NIR2}}$) achieved the highest values of Kappa in comparison with other NDWIs. The accuracy results of Wuhan WorldView-2 data are demonstrated in Table 5, where the $\text{NDWI}_{\text{green-NIR2}}$ and $\text{NDWI}_{\text{coastal-NIR2}}$ obtained better accuracy performance than other NDWIs.

Moreover, in order to further validate the results, we compare the false alarm rate (FPR) of different NDWIs when keeping the correctness rate (TPR) value equal to 90%. In this case, lower FPR

Table 3. Accuracy scores of various NDWIs for Shenzhen WorldView-2 data.

| NDWIs | | High-reflective band (ρ_h) | | | | | |
		Coastal	Blue	Green	Yellow	avg1	Average Kappa
Low-reflective band (ρ_l)	Red-edge	.538	.448	.504	.429	.500	.484
	NIR1	.586	.529	.559	.430	.538	.528
	NIR2	**.669**	.606	.652	.549	.622	.620
	avg2	.607	.549	.588	.491	.567	.560
Average Kappa		.600	.533	.576	.475	.557	
NDWI_sum		Kappa coefficient = .564					

Note: The bold value indicates the highest accuracy score.

values correspond to small false alarm and better performance. The results of the three study areas are shown in Tables 6–8, respectively. From the tables, a similar phenomenon can be observed that the NDWI$_{coastal-NIR2}$ and NDWI$_{green-NIR2}$ achieved the best performance with the lowest FPR value. Especially for Shenzhen WorldView-2 data, the NDWI$_{coastal-NIR2}$ reduced the FPR by 4.5% compared to the NDWI$_{green-NIR1}$. In addition, the average Kappa values and FPR values for each band were also calculated, and the NIR2 band surpassed other bands in terms of their highest accuracies and lowest FPR values, suggesting the NIR2 band plays an important role in the water extraction of WorldView-2 imagery. Consequently, the NDWI$_{coastal-NIR2}$ or NDWI$_{green-NIR2}$ can be selected as the optimized NDWI (NDWI$_{optimal}$) for WorldView-2 imagery considering the both indexes have the potential for enhancing the separability of water and non-water pixels.

Although the NDWI$_{optimal}$ can achieve the highest water extraction accuracy among all the possible band combinations of WorldView-2 imagery, it fails to remove the false alarms caused by shadow areas due to their high similarity to water in the spectral reflectance. After integrating the shadow index in this study, quantitative accuracies of the experimental results are reported in Tables 9–11. For Shenzhen WorldView-2 data, compared to the NDWI$_{optimal}$, the NDWI-MSI increases the PA and UA by 26.2% and 8.5%, respectively, by courtesy of the MSI index. Moreover, the Kappa coefficient increases from .669 to .863, which indicates the proposed method is more effective for discrimination between water and background, especially by reducing the commission errors of shadow. This phenomenon can be supported by the accuracy results of Hangzhou and Wuhan World-View-2 data (Tables 10 and 11), where the NDWI-MSI surpassed the optimal NDWI in terms of accuracies.

In order to further validate the proposed water index, some state-of-the-art supervised classification methods (e.g. MLC and SVM) were also carried out for the purpose of comparison. A grid-search technique using fivefold cross-validation was used to seek the optimal parameters of SVM with the RBF kernel. Specifically, 1000 water pixels and 1000 non-water pixels were randomly generated from the ground truth reference for training the two supervised classifiers, and the rest of samples were used for accuracy assessment. From the Table 9, it can be seen that the Kappa value of the proposed method surpassed MLC and SVM by .36 and .16, respectively. The accuracy results of Hangzhou and Wuhan (Tables 10 and 11) also show that the NDWI-MSI obtained better performance than the two classifiers. It should be kept in mind that MLC and SVM are performed on training samples but the proposed water index does not need sample collection.

Table 4. Accuracy scores of various NDWIs for Hangzhou WorldView-2 data.

| NDWIs | | High-reflective band (ρ_h) | | | | | |
		Coastal	Blue	Green	Yellow	avg1	Average Kappa
Low-reflective band (ρ_l)	Red-edge	.942	.943	.933	.965	.948	.946
	NIR1	.901	.935	.965	.960	.958	.944
	NIR2	**.966**	.957	**.966**	.961	.960	.962
	avg2	.943	.916	.965	.965	.960	.950
Average Kappa		.938	.938	.957	.963	.957	
NDWI_sum		Kappa coefficient = .962					

Note: The bold value indicates the highest accuracy score.

Table 5. Accuracy scores of various NDWIs for Wuhan WorldView-2 data.

NDWIs		High-reflective band (ρ_h)					Average Kappa
		Coastal	Blue	Green	Yellow	avg1	
Low-reflective band (ρ_l)	Red-edge	.776	.782	.852	.879	.826	.823
	NIR1	.884	.899	.956	.935	.918	.918
	NIR2	.969	.941	**.975**	.968	.962	.963
	avg2	.884	.905	.960	.953	.930	.926
Average Kappa		.878	.882	.936	.934	.909	
NDWI_sum		Kappa coefficient = .968					

Note: The bold value indicates the highest accuracy score.

Furthermore, the results of MLC and SVM were refined with the MSI feature (called MLC-MSI and SVM-MSI), in order to suppress the false alarms caused by the shadow areas. Accordingly, the MLC-MSI and SVM-MSI improved the water extraction accuracies compared to the original MLC and SVM. This results shows that the MSI-based shadow removal is also essential for the supervised water extraction. The NDWI-MSI achieved the comparable accuracies with SVM-MSI and MLC-MSI.

The extracted water maps of Shenzhen WorldView-2 data are displayed for a visual inspection in Figure 4. In order to show the detailed information, three representative areas were selected for comparison. It can be seen that some water bodies are omitted in the NDWI$_{optimal}$ (b). Most of the errors of MLC (d) and SVM (e) are related to the urban shadow. As observed in (c) and (f), the proposed method and SVM-MSI achieved the most satisfactory water body maps, due to the removal of shadow areas. The maps of water body extraction for Hangzhou and Wuhan (Figures 5 and 6) show similar conclusions to the results of the Shenzhen data. It can be found that the high water extraction accuracies achieved by the NDWI-MSI and SVM-MSI are consistent to the visual results (Figures 5 (c), (f) and 6(c), (f)), where the false alarms caused by shadow areas are less than other methods.

5. Discussions

In the study, various NDWIs constructed by possible band combinations of eight-band WorldView-2 data were tested, and the optimal NDWI (NDWI$_{coastal-NIR2}$ or NDWI$_{green-NIR2}$) was obtained according to the accuracy results of water extraction from the three test data. To further validate the reasonability of the results, the spectral response curves of various land cover classes in World-View-2 imagery are presented in Figure 7, where it can be seen that water absorbs strongly energy at NIR band and has a relatively high reflectance in coastal and green bands. Therefore, similar to the principle of the traditional water indexes (McFeeters 1996; Xu 2006), the NDWI$_{optimal}$ can be calculated by the normalized ratio of the high-reflectance band (coastal or green) and the low-reflectance band to separate water pixels from non-water pixels. Moreover, the distributions of the reflectance values (red-edge, NIR1, and NIR2) in the land cover types are presented in the following box plots (Figure 8). It can be found that the overlap between water and non-water (indicated by dotted lines) in the NIR2 band is smaller than that in the red-edge and NIR1 bands. In addition, the existing literature has reported that the coastal signature is the least absorbed by water in contrast to other

Table 6. FPR of various NDWIs when keeping the correctness rate (TPR) value equal to 90% for Shenzhen WorldView-2 data.

NDWIs		High-reflective band (ρ_h)					Average FPR (%)
		Coastal (%)	Blue (%)	Green (%)	Yellow (%)	avg1 (%)	
Low-reflective band (ρ_l)	Red-edge	10.2	14.8	14.8	43.0	15.0	19.6
	NIR1	7.1	9.2	9.3	25.0	9.6	12.0
	NIR2	**4.8**	6.1	5.9	13.5	6.0	7.3
	avg2	6.5	8.6	8.2	24.3	8.6	11.2
Average FPR		7.2	9.7	9.6	26.5	9.8	
NDWI_sum		FPR = 8.4%					

Note: The bold value indicates the lowest false alarm rate.

Table 7. FPR of various NDWIs when keeping the correctness rate (TPR) value equal to 90% for Hangzhou WorldView-2 data.

NDWIs		High-reflective band (ρ_h)					
		Coastal (%)	Blue (%)	Green (%)	Yellow (%)	avg1 (%)	Average FPR (%)
Low-reflective band (ρ_l)	Red-edge	2.5	2.4	0.5	0.1	1.3	1.4
	NIR1	1.2	0.7	0.1	0.2	0.2	0.5
	NIR2	0.1	0.1	0.1	0.1	0.1	0.1
	avg2	1.4	0.9	0.1	0.1	0.2	0.5
Average FPR		1.3	1.0	0.2	0.1	0.4	
NDWI_sum					FPR = 0.1%		

Table 8. FPR of various NDWIs when keeping the correctness rate (TPR) value equal to 90% for Wuhan WorldView-2 data.

NDWIs		High-reflective band (ρ_h)					
		Coastal (%)	Blue (%)	Green (%)	Yellow (%)	avg1 (%)	Average FPR (%)
Low-reflective band (ρ_l)	Red-edge	6.4	6.1	3.7	2.8	4.8	4.8
	NIR1	3.5	2.8	0.8	1.5	2.0	2.1
	NIR2	0.7	1.4	**0.6**	0.7	0.8	0.8
	avg2	3.5	2.9	0.8	1.0	2.1	2.1
Average FPR		3.5	3.3	1.5	1.5	2.4	
NDWI_sum					FPR = 0.8%		

Note: The bold value indicates the lowest false alarm rate.

Table 9. The accuracies of water extraction for Shenzhen WorldView-2 data set.

Methods	PA (%)	UA (%)	Kappa
NDWI	59.4	79.5	.669
NDWI-MSI	85.6	88.0	.863
MLC	95.9	36.7	.503
SVM	92.7	58.4	.702
MLC-MSI	90.9	77.1	.827
SVM-MSI	88.3	88.9	.881

**Table 10.** The accuracies of water extraction for Hangzhou WorldView-2 data set.

Methods	PA (%)	UA (%)	Kappa
NDWI	97.1	96.3	.966
NDWI-MSI	99.1	97.1	.977
MLC	98.1	89.3	.919
SVM	98.0	97.6	.972
MLC-MSI	98.1	98.2	.978
SVM-MSI	98.0	99.2	.982

Table 11. The accuracies of water extraction for Wuhan WorldView-2 data set.

Methods	PA (%)	UA (%)	Kappa
NDWI	98.6	97.1	.975
NDWI-MSI	99.9	99.4	.996
MLC	96.1	93.8	.940
SVM	99.2	92.8	.951
MLC-MSI	96.1	99.9	.977
SVM-MSI	99.2	99.9	.995

bands (Anderson and Marchisio 2012), and it is expected to be useful for water research and bathymetric studies (Puetz, Lee, and Olsen 2009).

NDWI$_{optimal}$ may still suffer from the effects of shadow noise despite its higher accuracies in comparison to other NDWIs. The index values of NDWI$_{green-NIR1}$, NDWI$_{green-NIR2}$, NDWI$_{coastal-NIR2}$, and NDWI-MSI in the major land cover types are presented in Figure 9, respectively. As shown
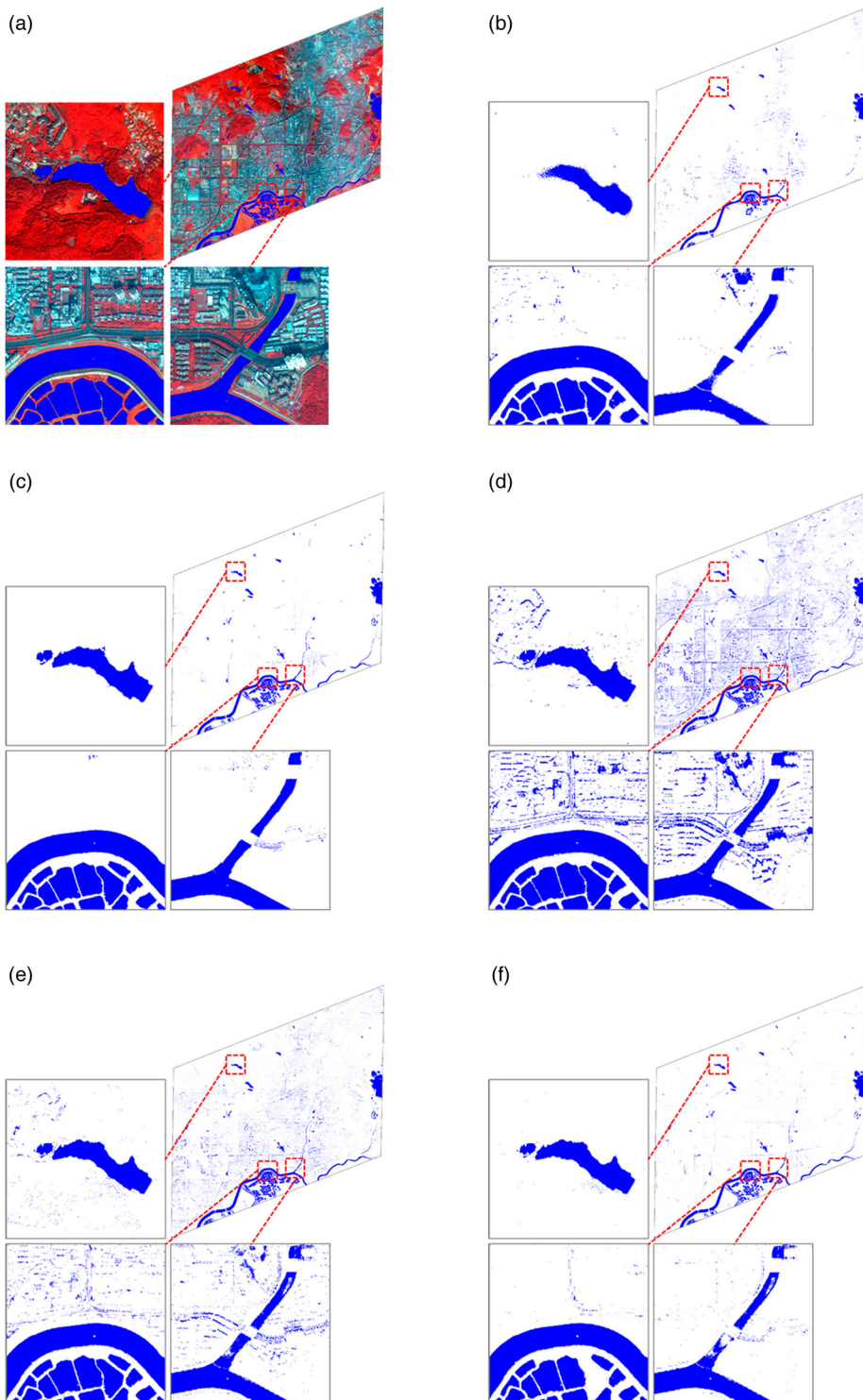
Figure 4. Results of water extraction for Shenzhen WorldView-2 data set: (a) false color image (8, 3, and 2) overlaid with ground truth reference; (b) NDWI; (c) proposed method; (d) MLC; (e) SVM; and (f) SVM-MSI.
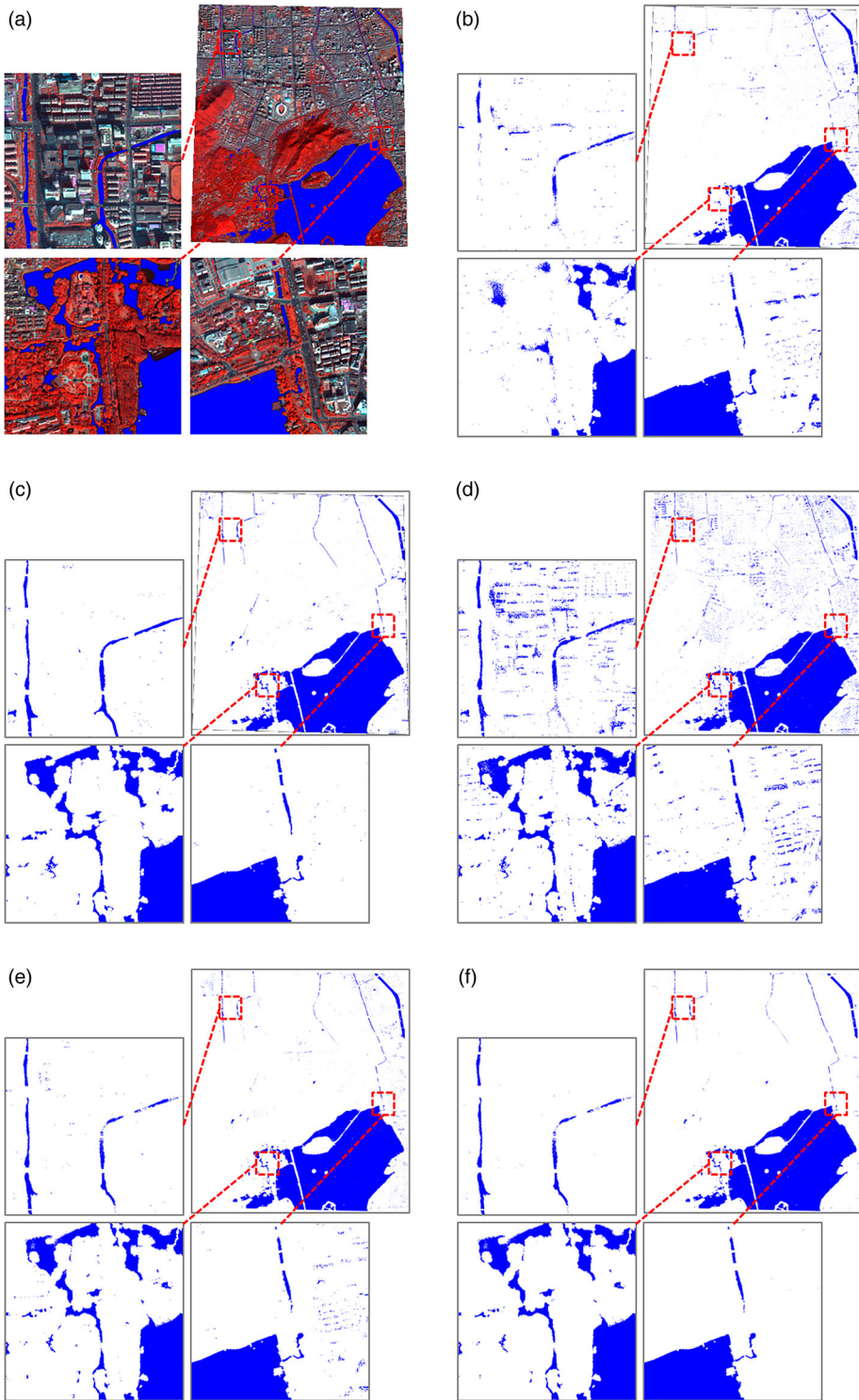
Figure 5. Results of water extraction for Hangzhou WorldView-2 data set: (a) false color image (8, 3, and 2) overlaid with ground truth reference; (b) NDWI; (c) proposed method; (d) MLC; (e) SVM; and (f) SVM-MSI.
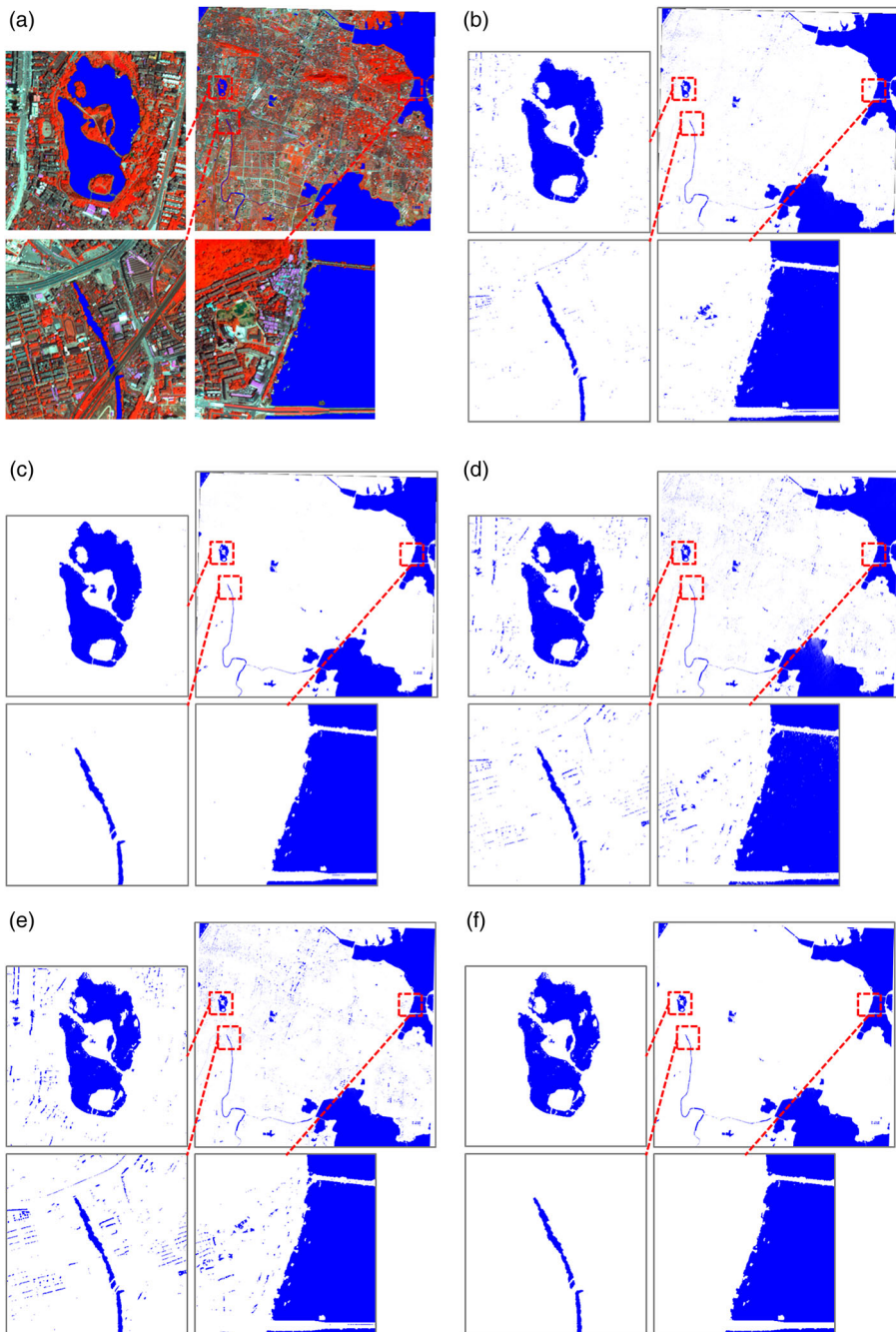
Figure 6. Results of water extraction for Wuhan WorldView-2 data set: (a) false color image (8, 3, and 2) overlaid with ground truth reference; (b) NDWI; (c) proposed method; (d) MLC; (e) SVM; and (f) SVM-MSI.

in the figure, there are overlaps in the three NDWIs values between water and shadow (a–c), which indicates the NDWIs cannot completely distinguish water from shadow pixels, especially for high-resolution imagery. Therefore, MSI is introduced to the new water index, in order to eliminate the false alarms caused by shadow (d).
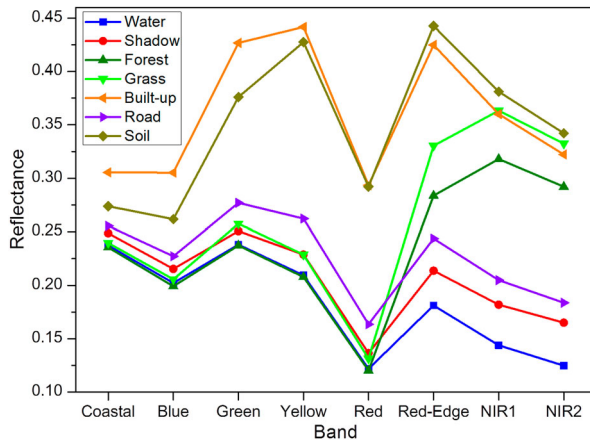
Figure 7. Spectral responses of various land cover classes in eight-band WorldView-2 imagery.
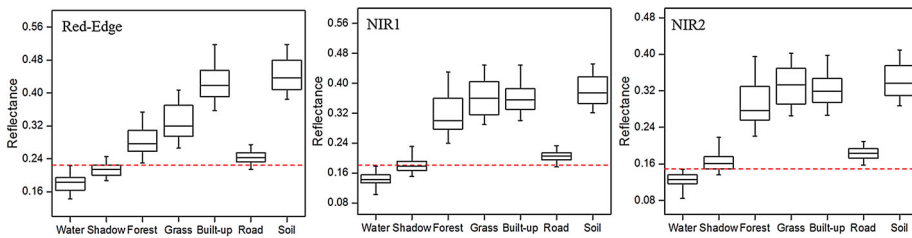
Figure 8. Reflectance distributions of various land cover classes. Each box plot shows the location of the 5th, 25th, 50th, 75th, and 95th percentiles using horizontal lines (boxes and whiskers).

In addition, selection of an appropriate threshold value for the water index has an important impact on the water extraction results. The threshold values vary with the complicated environmental conditions and various imaging conditions. In urban high-spatial resolution imagery, the presence of shadow areas cast by buildings and trees is the primary noise source affecting the selection of threshold values. In this research, the MSI was introduced to suppress the effects of shadow, and NDWI-MSI was constructed to maximize the separability of water and non-water features. Therefore, a peak-valley method of histogram segmentation scheme (Julie et al. 2007) is used for threshold selection of the new index.

In the experiments, the three WorldView-2 images with various urban environments and surface water conditions were used to test the new water index, and satisfactory results of water extraction were achieved in all the cases. However, it should be noted that the influence of seasonal variations or biochemical property of water bodies on the reflectance response of surface water cannot be ignored, which may affect the performance of the new water index and accuracies of water extraction.

6. Conclusions

In this paper, we proposed a novel water index for high-resolution WorldView-2 imagery combining a new NDWI and MSI, which is able to delineate accurately water bodies and simultaneously suppress the false alarms caused by shadow areas. Firstly, in order to develop adequately the potential of the WorldView-2 bands, various NDWIs were computed by possible combinations of the eight-band data. The NDWI constructed by the normalized ratio of coastal-NIR2 or green-NIR2 bands outperformed other NDWIs in terms of the accuracies of water extraction. The commission errors of water
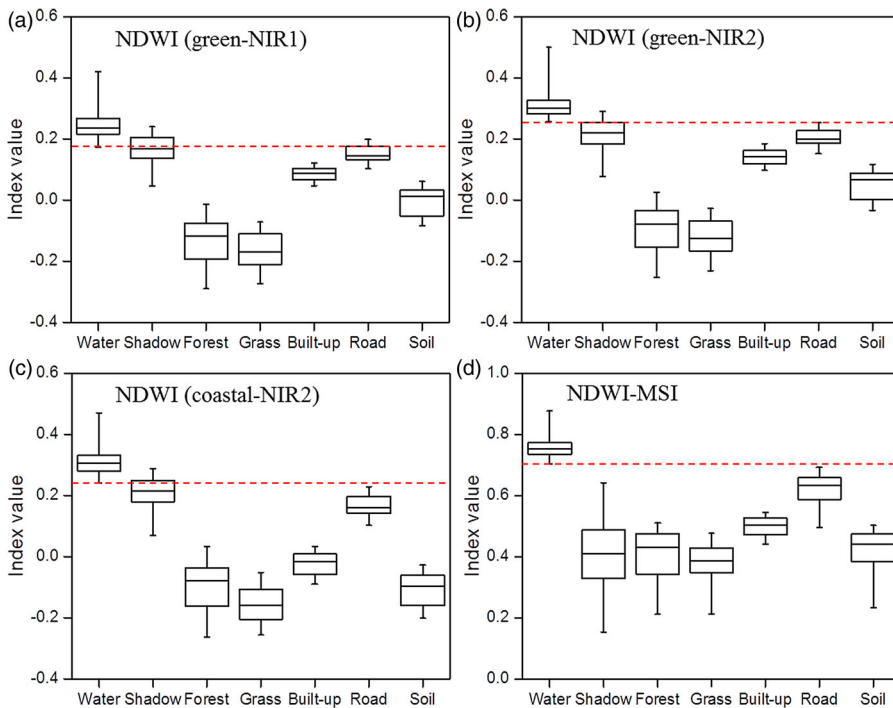
Figure 9. Index distributions of major land cover types. Each box plot shows the location of the 5th, 25th, 50th, 75th, and 95th percentiles using horizontal lines (boxes and whiskers).

extraction are mainly related to shadow areas due to their similar spectral characteristics. Thus, MSI was used to eliminate the noise caused by shadow. Three WorldView-2 data sets covering Shenzhen, Hangzhou, and Wuhan were used to validate the effectiveness of the proposed method. The experimental results revealed that the accuracy scores of the new index were higher than the original NDWI, and the NDWI-MSI was able to effectively reduce false alarms in terms of the visual inspection. Moreover, compared with the supervised machine learning algorithms (e.g. MLC and SVM), the NDWI-MSI achieved higher accuracy and also showed significant superiority. In general, the proposed water index is an effective water extraction method, which can be applicable as a routine tool for water body detection and monitoring for high-resolution images.

Disclosure statement

No potential conflict of interest was reported by the authors.

Funding

References

Anderson, Neal T., and Giovanni B. Marchisio. 2012. "WorldView-2 and the Evolution of the DigitalGlobe Remote Sensing Satellite Constellation: Introductory Paper for the Special Session on WorldView-2." In *Algorithms and Technologies for Multispectral, Hyperspectral, and Ultraspectral Imagery XVIII, 83900L*. Proc. SPIE, edited by Sylvia S. Shen and Paul E. Lewis. Baltimore, MD: Spie Digital Library.

Bryant, R. G., and M. P. Rainey. 2002. "Investigation of Flood Inundation on Playas Within the Zone of Chotts, Using a Time-series of AVHRR." *Remote Sensing of Environment* 82 (Suppl. 2–3): 360–375.

Carroll, M. L., J. R. Townshend, C. M. DiMiceli, P. Noojipady, and R. A. Sohlberg. 2009. "A New Global Raster Water Mask at 250 M Resolution." *International Journal of Digital Earth* 2 (4): 291–308.

Chapelle, O., P. Haffner, and V. N. Vapnik. 1999. "Support Vector Machines for Histogram-based Image Classification." *IEEE Transactions on Neural Networks* 10 (5): 1055–1064.

Chen, Chen, Jing Xin Chen, L. I. Xiang-Qian, Qin Zhang, and Shu Qian Zheng. 2013. "Study on Water Body Information Extraction from High Resolution Remote Sensing Image Based on Object-oriented Method." *Yellow River* 35 (9): 68–70 + 73.

Craglia, Max, Kees de Bie, Davina Jackson, Martino Pesaresi, Gábor Remetey-Fülöpp, Changlin Wang, Alessandro Annoni, Ling Bian, Fred Campbell, and Manfred Ehlers. 2012. "Digital Earth 2020: Towards the Vision for the Next Decade." *International Journal of Digital Earth* 5 (1): 4–21.

Famiglietti, James S., and Matthew Rodell. 2013. "Water in the Balance." *Science* 340 (6138): 1300–1301.

Fawcett, Tom. 2006. "An Introduction to ROC Analysis." *Pattern Recognition Letters* 27 (8): 861–874.

Feng, Min, Joseph O. Sexton, Saurabh Channan, and John R. Townshend. 2015. "A Global, High-resolution (30-M) Inland Water Body Dataset for 2000: First Results of a Topographic–Spectral Classification Algorithm." *International Journal of Digital Earth* 9 (2): 113–133.

Feyisa, Gudina L., Henrik Meilby, Rasmus Fensholt, and Simon R. Proud. 2014. "Automated Water Extraction Index: A New Technique for Surface Water Mapping Using Landsat Imagery." *Remote sensing of Environment* 140 (1): 23–35.

Gotsis, P. K., C. C. Chamis, and L. Minnetyan. 2004. "Classification of Hyperspectral Remote Sensing Images with Support Vector Machines." *IEEE Transactions on Geoscience and Remote Sensing* 42 (8): 1778–1790.

Huang, C., L. S. Davis, and J. R. G. Townshend. 2002. "An Assessment of Support Vector Machines for Land Cover Classification." *International Journal of Remote Sensing* 23 (4): 725–749.

Huang, Xin, and Liangpei Zhang. 2012. "Morphological Building/Shadow Index for Building Extraction from High-resolution Imagery over Urban Areas." *IEEE Journal of Selected Topics in Applied Earth Observations and Remote Sensing* 5 (1): 161–172.

Jain, Sanjay K., R. D. Singh, M. K. Jain, and A. K. Lohani. 2005. "Delineation of Flood-prone Areas Using Remote Sensing Techniques." *Water Resources Management* 19 (4): 333–347.

Ji, L., L. Zhang, and B. Wylie. 2009. "Analysis of Dynamic Thresholds for the Normalized Difference Water Index." *Photogrammetric Engineering & Remote Sensing* 75 (11): 1307–1317.

Jiang, Hao, Min Feng, Yunqiang Zhu, Ning Lu, Jianxi Huang, and Tong Xiao. 2014. "An Automated Method for Extracting Rivers and Lakes from Landsat Imagery." *Remote Sensing* 6 (6): 5067–5089.

Julie, Delon, Desolneux Agnès, Lisani José-Luis, and Petro Ana Belén. 2007. "A Nonparametric Approach for Histogram Segmentation." *Image Processing IEEE Transactions on* 16 (1): 253–261.

Li, Jiang, and Ram M. Narayanan. 2003. "A Shape-based Approach to Change Detection of Lakes Using Time Series Remote Sensing Images." *IEEE Transactions on Geoscience and Remote Sensing* 41 (11): 2466–2477.

Li, Changchun, Guangsheng Zhang, and Li Shen. 2013. "Water Body Extraction from Remote Sensing Image Based on AdaBoost Algorithm." *Science of Surveying and Mapping* 38 (2): 104–000.

Liao, An Ping, Li Jun Chen, Jun Chen, H. E. Chaoying, Xin Cao, Jin Chen, Shu Peng, Fang Di Sun, and Peng Gong. 2014. "High-resolution Remote Sensing Mapping of Global Land Water." *Science China Earth Sciences* 57 (10): 2305–2316.

Lira, Jorge. 2006. "Segmentation and Morphology of Open Water Bodies from Multispectral Images." *International Journal of Remote Sensing* 27 (18): 4015–4038.

Luo, Jiancheng, Sheng Yongwei, Shen Zhanfeng, and Li Junli. 2010. "High-precise Water Extraction Based on Spectral-spatial Coupled Remote Sensing Information." *In 2010 IEEE International Geoscience and Remote Sensing Symposium (IGARSS)*, 2840–2843. http://ieeexplore.ieee.org/xpls/abs_all.jsp?arnumber=5648978&tag=1

McFeeters, S. K. 1996. "The Use of the Normalized Difference Water Index (NDWI) in the Delineation of Open Water Features." *International Journal of Remote Sensing* 17 (7): 1425–1432.

Nath, Rajiv Kumar, and S. K. Deb. 2010. "Water-Body Area Extraction from High Resolution Satellite Images-An Introduction, Review, and Comparison." *International Journal of Image Processing* 3 (6): 353–372.

Nettleman, M. D. 1988. "Receiver Operator Characteristic (ROC) Curves." *Infection Control & Hospital Epidemiology the Official Journal of the Society of Hospital Epidemiologists of America* 9 (8): 374–377.

Puetz, Angela M., Krista Lee, and R. Chris Olsen. 2009. "WorldView-2 Data Simulation and Analysis Results." *Proceedings of SPIE – The International Society for Optical Engineering*, 73340U-U-9.

Rogers, A. S., and M. S. Kearney. 2004. "Reducing Signature Variability in Unmixing Coastal Marsh Thematic Mapper Scenes Using Spectral Indices." *International Journal of Remote Sensing* 25 (12): 2317–2335.

Ryu, Joo Hyung, Joong Sun Won, and Kyung Duck Min. 2002. "Waterline Extraction from Landsat TM Data in a Tidal Flat – A Case Study in Gomso Bay, Korea." *Remote Sensing of Environment* 83 (3): 442–456.

Strahler, Alan H. 1980. "The Use of Prior Probabilities in Maximum Likelihood Classification of Remotely Sensed Data." *Remote Sensing of Environment* 10 (2): 135–163.

Sun, Fangdi, Wanxiao Sun, Jin Chen, and Peng Gong. 2012. "Comparison and Improvement of Methods for Identifying Waterbodies in Remotely Sensed Imagery." *International Journal of Remote Sensing* 33 (21): 6854–6875.

Wolf, Antonio F. 2012. "Using WorldView-2 Vis-NIR Multispectral Imagery to Support Land Mapping and Feature Extraction Using Normalized Difference Index Ratios." *Society of Photo-Optical Instrumentation Engineers (SPIE) Conference Series*, 8390.

Xu, H. Q. 2006. "Modification of Normalised Difference Water Index (NDWI) to Enhance Open Water Features in Remotely Sensed Imagery." *International Journal of Remote Sensing* 27 (14): 3025–3033.

Zhou, Yanan, Jiancheng Luo, Zhanfeng Shen, Xi Cheng, and Xiaodong Hu. 2012. "Adaptive Extraction of Water in Urban Areas Based on Local Iteration Using High-Resolution Multi-Spectral Image." *In 2012 IEEE International Geoscience and Remote Sensing Symposium (IGARSS)* 53 (60): 6024–6027.